Advances in Natural Sciences:
Nanoscience and Nanotechnology

Iron oxide-based conjugates for cancer theragnostics

OPEN ACCESS
IOP PUBLISHING
ADVANCES IN NATURAL SCIENCES: NANOSCIENCE AND NANOTECHNOLOGY
Adv. Nat. Sci.: Nanosci. Nanotechnol. **3** (2012) 033001 (13pp)
doi:10.1088/2043-6262/3/3/033001

REVIEW

Iron oxide-based conjugates for cancer theragnostics

Xuan Phuc Nguyen[1], Dai Lam Tran[1], Phuong Thu Ha[1], Hong Nam Pham[1], Thu Trang Mai[1], Hoai Linh Pham[1], Van Hong Le[1], Hung Manh Do[1], Thi Bich Hoa Phan[1], Thi Ha Giang Pham[2], Dac Tu Nguyen[2], Thi My Nhung Hoang[2], Khanh Lam[3] and Thi Quy Nguyen[2]

[1] Laboratory of Biomedical Nanomaterials, Institute of Materials Science, Vietnam Academy of Science and Technology, 18 Hoang Quoc Viet Road, Cau Giay district, Hanoi, Vietnam
[2] Faculty of Biology, Hanoi University of Science, 334 Nguyen Trai street, Hanoi, Vietnam
[3] High Technology Center, Central Military Hospital No. 108, 1 Tran Hung Dao, Hanoi, Vietnam

E-mail: phucnx@ims.vast.ac.vn

Received 26 February 2012
Accepted for publication 12 March 2012
Published 1 June 2012
Online at stacks.iop.org/ANSN/3/033001

Abstract
In this paper we first summarize our recent research on fabrication and structure characterization of conjugates of Fe_3O_4 nanoparticles (MNPs) encapsulated by several organic materials such as oleic acid (OL), starch (ST), dextran (D), chitosan (CS), O-carboxymethyl chitosan (OCMCS) and the copolymer of poly(styrene-co-acrylic acid (St-co-AA)). The ferrofluids stability and toxicity were also considered. The magnetic inductive heating (MIH) curves were measured using a set up with an alternating (ac) magnetic field of strength of 40–100 Oe and frequency of 180–240 kHz. We then present new results dealing with attempting to apply the MNP/copolymer ferrofluid for treatment of Sarcoma 180 tumor. *In vitro* as well as *ex vivo* MIH experiments were carried out as preparation steps in order to estimate the proper conditions for the *in vivo* MIH experiment. As for the latter, we have successfully carried out the treatment of solid tumor of size around 6 × 6 mm inoculated on Swiss mice with use of a dose of 0.3–0.4 mg ml^{-1} ferrofluid injected subcutaneously into the tumor and field-irradiated for 30 min. Two groups of treated mice recovered in three weeks from MIH treatment three times during the first week. We finally show that curcumin loaded MNP-based conjugates showed themselves to be a potential agent for application as a bimodal contrast enhancer of magnetic resonance imaging (MRI) and fluorescence imaging. Additionally, *in vitro* and *ex vivo* studies by these two techniques evidenced that macrophage is capable of uptake and tends to carry the MNPs into a tumor.

Keywords: magnetic nanoparticles, drug delivery, cancer, *in vivo* hyperthermia, curcumin, macrophage

Classification numbers: 4.02, 5.02

1. Introduction

One of main tasks of nanomedicine is to fabricate drug delivery and imaging nanovectors, which are the multifunctional nanoparticles containing both in-core therapeutic elements like drugs, contrast enhancer, permeation enhancer as well as on-surface biological modifiers such as targeting moiety, polyethylene glycol [1]. Among various core materials [1–3], magnetic nanoparticles (MNPs) have important advantages due mainly to the three following

properties (see e.g. review papers [2, 4]). Firstly, the unique ability of MNPs to be guided by an external magnetic field has been utilized for targeted drug and gene delivery, tissue engineering, cell tracking and bioseparation. Secondly, with the ability to perturb magnetic local field, they can serve as effective contrast enhancer in magnetic resonance imaging (MRI). Finally, MNPs can effectively adsorb energy from external alternating magnetic field to create a nanosized heating source that is used as thermoseed in magnetic inductive heating (MIH) hyperthermia. The combination of the first with the second and/or the third application makes MNPs, in fact, a multifunctional nanovector. Up to now, several MNP-based nanovectors have been designed and fabricated with the use of different magnetic materials for the core as well as various materials for the capping [5–9]. Although new magnetic materials such as exchanged-coupled $CoFe_2O_4$@$MnFe_2O_4$ core-shell [8] and FeCo [9] nanoparticles have recently been shown to be promising candidates for biomedical applications, iron oxide-based nanoconjugates are most widely investigated for using in MRI diagnosis [4, 10–13] and hyperthermia treatment [4, 10, 11, 14–17] of cancer.

In this paper we will first summarize the results recently achieved by the Laboratory of Biomedical Nanomaterials in fabrication of Fe_3O_4 magnetic nanoparticles encapsulated with different organic materials [18–24]. The preliminary study to apply the MNPs capped with a synthesized copolymer for hyperthermia will be presented. The loading of curcumin onto the MNPs will be, finally, shown to demonstrate a possibility to fabricate a drug delivery system with more than two functions.

2. Experimental

2.1. Fabrication

2.1.1. Materials. All the chemicals used were of reagent grade. Ferric chloride hexa-hydrate ($FeCl_3 \cdot 6H_2O$), ferrous chloride tetra-hydrate ($FeCl_2 \cdot 4H_2O$), sodium hydroxide (NaOH), ammonia (NH_3), hydrochloric acid (HCl), acetone ($(CH_3)_2CO$), acrylic acid (AA), styrene (St), ammonium persulfate ($(NH_4)_2S_2O_8$) and oleic acid (OL) were purchased from Aldrich and used without further purification. Chitosan (CS) with molecular weight of 400 000 and degree of acetylation of 70% was received from Nha Trang Aquatic Institute (Vietnam) and characterized by infrared (IR) spectroscopy and viscometry measurements. Curcumin (Cur) (chemical name: 1,7-bis(4-hydroxy-3-methoxyphenyl)-1,6-heptadiene-3,5-dione) was provided by the Institute of Chemistry (Vietnam).

Cells were cultured in Roswell Park Memorial Institute (RPMI) 1640 medium (by Gibco). This medium was added with 10% fetal bovine serum (Invitrogen), 100 IU ml^{-1} penicillin-streptomycine (Invitrogen), 2 mM glatumine (Invitrogen). Cells were grown in a humidified chamber in the presence of 5% CO_2, at 37 °C. Human Buffy coat was received from the National Institute of Hematology and Transfusion (Vietnam). Mononuclear cells were isolated by density gradient centrifugation using 1.077 g ml^{-1} Ficoll. Cells were cultured in RPMI 1640 medium with 1 μg ml^{-1} of human granucocyte macrophage colony stimulating factor HGM-CSF (MPBiomedicals). 7–12 week-old Swiss mice were obtained from the National Institute of Hygiene and Epidemiology (Vietnam). Human monocyte or mouse primary peritoneal macrophages were grown for 24 h on glass coverslips. 10^6 cells were incubated with 0.05 mg MNPs for 2–15 h, then treated with either anti-human CD14 antibody (BioLegend) or actins antibody (Invitrogen) for taking laser scanning confocal microscope (LSCM) images.

2.1.2. Synthesis of curcumin loaded Fe_3O_4/oleic acid and Fe_3O_4/chitosan ferrofluids. OL-coated Fe_3O_4 and CS-coated Fe_3O_4 ferrofluids (OLF and CSF) were prepared by co-precipitation of Fe^3 and Fe^2 by NaOH in the presence of OL and CS, respectively. Briefly, OLF and CSF were synthesized by the co-precipitation from iron chloride solution (with Fe^{3+}/Fe^{2+} ratio of 2:1). Then, Cur (preliminarily solved in ethanol) was attached by adsorption on the Fe_3O_4 surface of the OLF and CSF. Several types of ferrofluid with and without Cur have been prepared for further fluorescent and magnetic imaging studies. More details of the synthesis procedure can be found in [21].

2.1.3. Synthesis of Fe_3O_4/poly(St/co-AA) ferrofluid. The Fe_3O_4/poly(St-co-AA) ferrofluid (named also as copolymer, or abbreviated as AAF) was prepared by both *ex situ* or *in situ* means depending on the capping process. In the *ex situ* approach, the Fe_3O_4 nanoparticles and poly(St-co-AA) were, correspondingly, co-precipitated and polymerized before they were mixed to form the core-shell Fe_3O_4/copolymer ferrofluid. In the *in situ* case, the encapsulating process was undertaken during the polymerization of poly(St-co-AA) in the presence of the readily made (by co-precipitation) Fe_3O_4 nanoparticles. The procedures are described in more detail in [22].

2.2. Characterization

The crystalline structure of Fe_3O_4 was determined by x-ray diffraction (XRD) equipment SIEMENS D-5000. Field emission scanning electron microscope (FE-SEM) and transmission electron microscope (TEM) images were analyzed by Hitachi S-4800 and JEM-1200EX equipment, respectively. The magnetic properties of the MNP powder and ferrofluids were determined by a homemade vibrating sample magnetometer (VSM) as well as a Quantum Design physical property measurement system (PPMS). The binding between the Fe_3O_4 core and the organic capping materials were characterized by use of infrared (IR) and ultraviolet-visible (UV–Vis) spectra, which were recorded with Nicolet 6700 Fourier transform infrared (FT-IR) spectrometer and UV–Vis Agilent 8453 spectrophotometer, correspondingly. The formation of the poly(St-co-AA) copolymer was studied additionally by proton nuclear magnetic resonance (^{1}H-NMR) on a 500 MHz Bruker spectrometer. Differential thermal analysis (DTA) was performed on a DT-60H and the fluorescence images were recorded by use of Zeis-510 LSCM microscope. Hydrodynamic diameters were characterized by dynamic light scattering (DLS) technique on a Malvern Zetasizer.

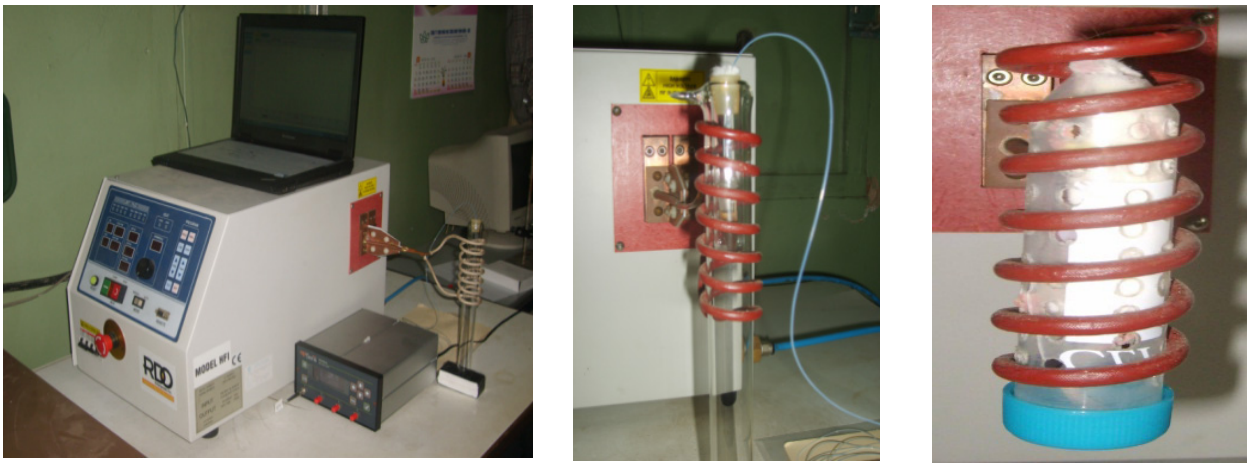

a *b* *c*

Figure 1. MIH experimental set-up.

2.3. In vitro *and* in vivo *hyperthermia experiments*

All the MIH experiments were carried out on the set up with the use of a commercial generator (RDO HFI 5 kW) providing an alternating magnetic field of amplitude from 40 to 100 Oe, and frequency of 180–240 kHz. The sample temperature was measured online by optical thermometer (Opsens). For characterization of the heating performance, ferrofluid samples of various particle concentrations (diluted in water) were prepared and kept in a round-bottom-shaped glass holder, so that the temperature sensor was imbedded directly in them. The same experimental arrangement was also applied for *in vitro* experiment while the sample was a mixture of ferrofluid with Sarcoma cells. *In vivo* hyperthermia experiment was designed for treatment of a Sarcoma tumor of size of around $6 \times 6\,\text{mm}^2$, which had been transplanted subcutaneously on Swiss mice. The mouse was introduced into a plastic tube of inner diameter of 30 mm, which then was inserted into a 10 turns coil of diameter of 30 mm. Figure 1 presents pictures of the used MIH set-up (a), and *in vitro* or *ex vivo* (b), and *in vivo* (c) sample arrangement.

3. Results and discussion

3.1. Ferrofluid characteristics

3.1.1. Structural characteristics of Fe_3O_4/AA, Fe_3O_4/OL *and* Fe_3O_4/CS. The XRD patterns of the co-precipitated Fe_3O_4 powder and of those of the dried ferrofluids (see e.g. on figure 2(a)) indicate that the samples are of single magnetite phase. The analysis of the XRD peaks (based on Scherrer method) as well as that of the FE-SEM images showed that the co-precipitated particles are of 15–20 nm in diameter. The size of the capped particles become enlarged, however, the mass analysis performed via thermogravimetric analysis (TGA) and magnetization for the case of chitosan and dextran materials showed that the weight contribution of the coating layer is as small as only about 5–10% (figure 2(b)). The hydrodynamic diameter of the ferrofluids, on the other hand, depends very much on both the capping materials and the chemicobiological condition of the fluid.

Figures 3 and 4 present the DLS size distribution curve (left) versus FE-SEM images (right) of OLF (upper) and OLF-Cur (bottom), and CSF (upper) and CSF-Cur (bottom) samples, respectively. The used solvent was water for all the ferrofluids. In all these samples, the FE-SEM clearly depicts spherical particles of diameter of tens of nanometers, which reflect the encapsulation of the magnetite nanoparticles. The loading of curcumin, as indicated by DLS curves, leads to formation of larger clusters. The preference of the cluster formation for the OL and CS ferrofluids is that, for the former case the clusters are clearly of ball shape with diameter of less than 300 nm, whereas in the latter case the clusters are supposed to be of matrix object of much larger size. The fact that OL-capped MNPs are much better monodisperse than those capped by CS is seen very clearly by the LSCM images, measured for the two ferrofluids loaded with curcumin, i.e. OLF-Cur and CSF-Cur (figure 5). This behavior can be understood by taking into account the fact that oleic acid, as a fatty acid, is a good surfactant agent. We then chose the OLF-Cur as a model drug delivery system for studying the uptake of the curcumin drug by macrophage to be observed by either fluorescence or magnetization methods (section 3). Figure 6 presents the ^{1}H-NMR spectra for the AA monomer (a), St monomer (b) and poly(St-co-AA) copolymer. The formation of the poly(St-co-AA) is confirmed by the change in ^{1}H-NMR spectra of the AA (bottom) and styrene (middle) monomer into that of the copolymer poly (St-co-AA) (upper). The $^1\text{H}-\text{NMR}$ peaks of the vinyl group appear at 6.52, 6.14 and 5.96 ppm for acrylic acid, and those at 6.69, 5.72 and 5.21 ppm for styrene totally disappear in the spectrum of the copolymer. Instead of this one observes broad peaks in the 3.31–2.30 and 2.09–1.20 ppm region. The formation of poly(St-co-AA) was confirmed also by IR spectra, where the vibration peaks of the copolymer were observed to summarize all those of the two monomers (figures not shown). On the spectrum of Fe_3O_4/poly(St-co-AA) (figure 7), the presence of free carboxyl group on the surface was verified from the observed C=O stretching band (1702 cm^{-1}) as well as a plateau of OH stretching band at co. 3015 cm^{-1}. The linking between Fe_3O_4 and the capping copolymer was evidenced by appearance of

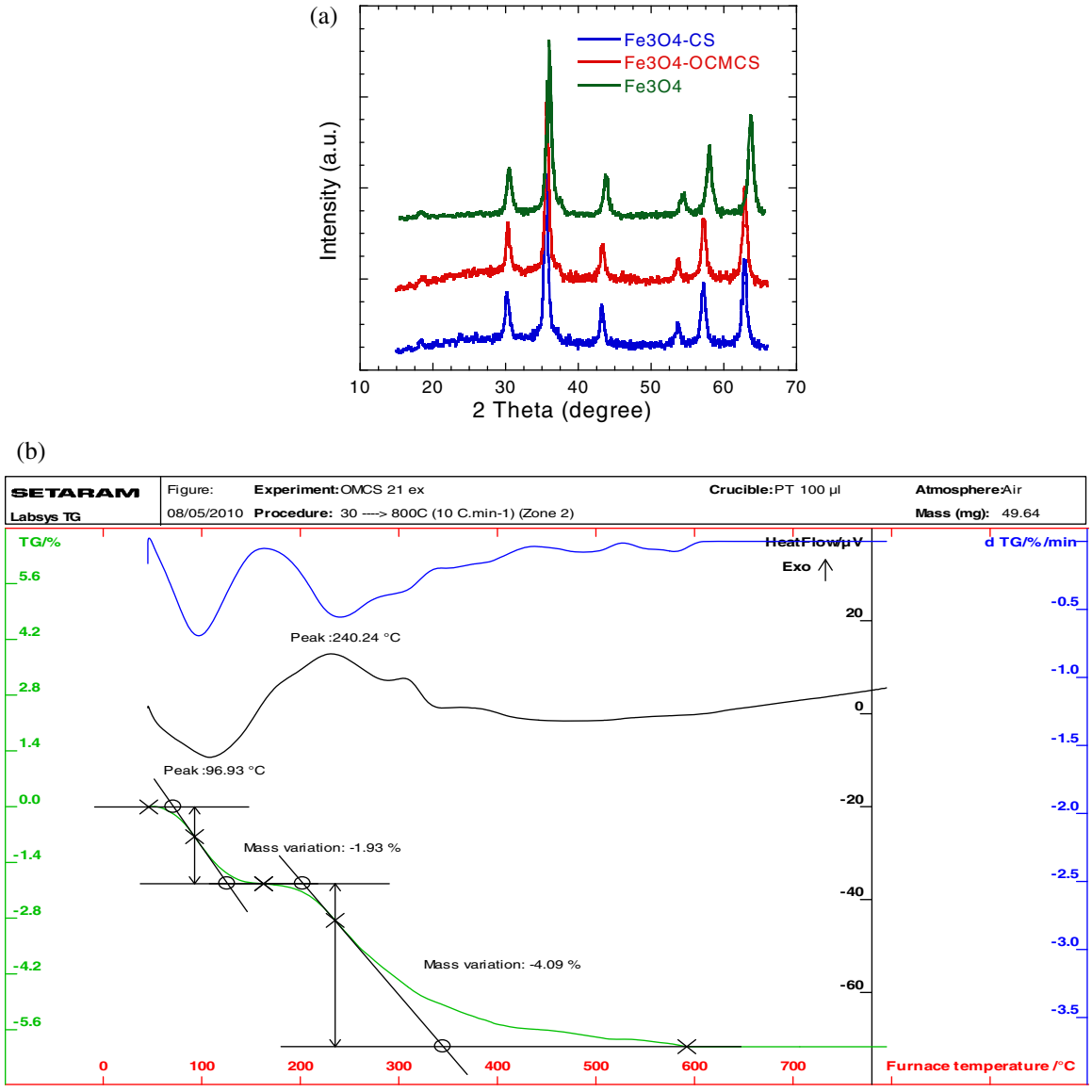

Figure 2. (a) XRD diagrams of naked, CS-coated and OCMCS-coated MNPs. (b) TGA curve for CS-coated Fe_3O_4.

peaks at 612 and 565 cm^{-1} (figure 7), which are assigned to the splitting, due to nanosized particle behavior, of the stretching Fe–O–Fe vibration originally observed at 585 cm^{-1} for the bulk Fe_3O_4 crystal. We therefore suggest that in order to make the Fe_3O_4/poly(St-co-AA) well soluble in water, the hydrophilic AA monomer should dominate by at least twice that of the hydrophobic St one.

3.1.2. Magnetic characteristics of conjugates. The magnetizations of the as-coprecipitated Fe_3O_4 powders of different syntheses were in the range of 65–70 emu g^{-1} (figure 8). Figure 8 shows also magnetization curves obtained for the dried samples of Fe_3O_4 nanoparticles encapsulated with chitosan and O-carboxymethyl chitosan. The observed very tiny decrease of magnetization, i.e. less than 5%, indicates that the capping procedures by wet chemistry have no impact on the magnetite structure of the magnetic particles. This observation is in good agreement with the XRD and TGA observation shown in figure 2. Figure 9 presents magnetizations of colloidal suspensions of MNP capped by various materials both with and without curcumin. As seen, the suspension magnetization depends very much on the type of encapsulating material which, in fact, can be classified into three groups. Firstly, oleic acid when used alone has provided very dilute MNP in-water suspension, namely with small magnetization of order of 0.1 emu g^{-1} (or emu ml^{-1}), corresponding to MNP concentration $c = 1.7$ mg ml^{-1}. Secondly, poly(St-co-AA) as amphiphilic copolymer can serve as a rather good encapsulating material, resulting in ferrofluid of magnetization of order of 0.65 emu g^{-1} (corresponding to $c = 9.1$ mg ml^{-1}). The third group, comprising of natural polymers such as starch, chitosan and O-carboxymethyl chitosan, formulated the conjugates of highest MNP concentration, namely with magnetization of order of 1.1 ± 0.1 emu g^{-1} ($c = 16.0 \pm 0.15$ mg ml^{-1}). This variation in MNP concentration, as large as of one order in value, is supposed to be related with different structures of the conjugates. We assume that due to strong amphiphilic property the single molecular OL and bimolecular St-co-AA materials can serve in providing spherical conjugates of from single to several tens of MNPs in core, whereas for the case

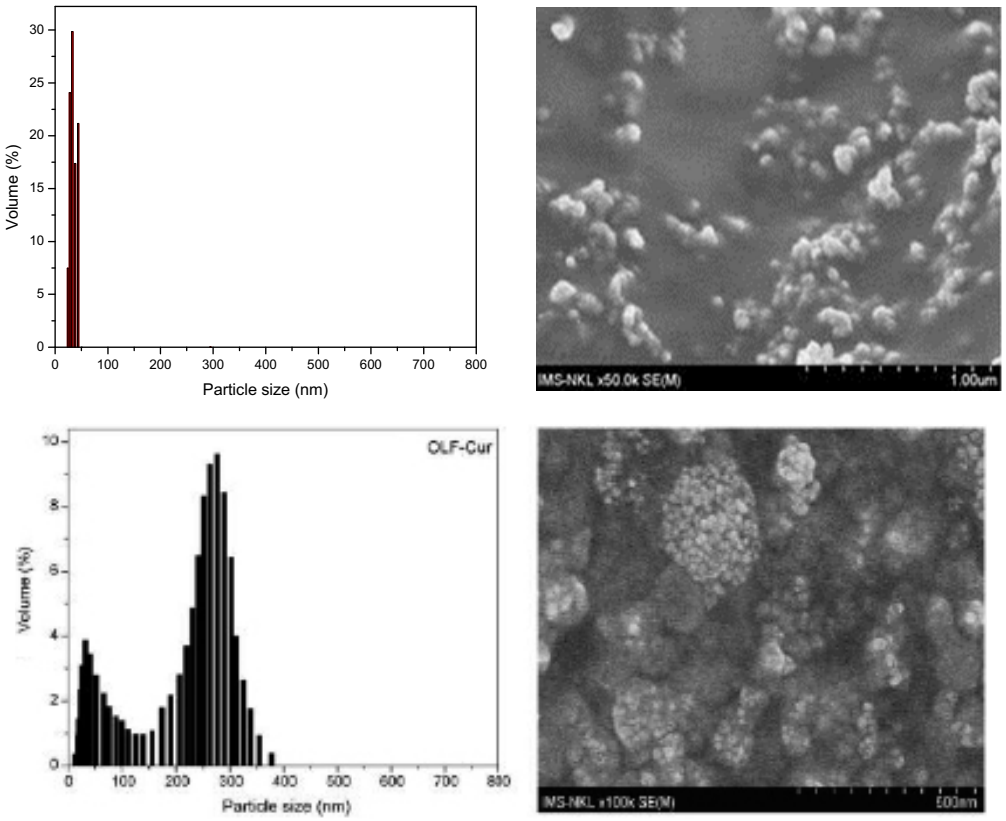

Figure 3. DLS (left) and FE-SEM image (right) of OLF (upper) and OLF-Cur (bottom) conjugates.

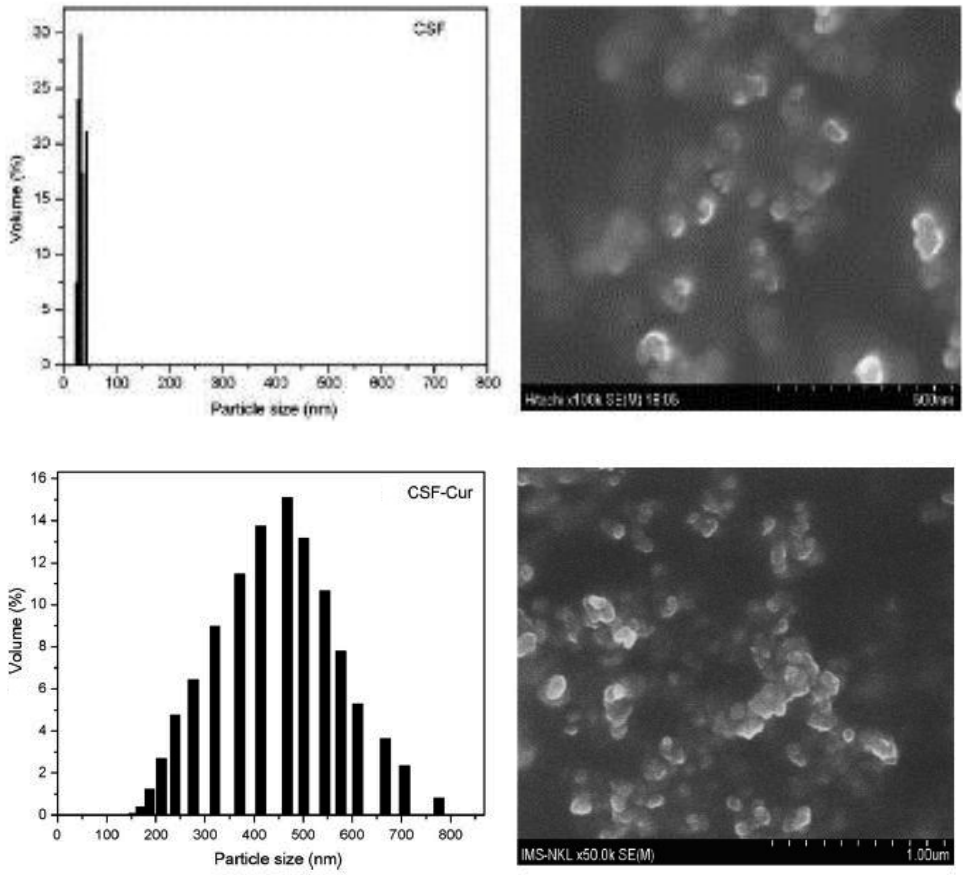

Figure 4. DLS (left) and FE-SEM image (right) of CSF (upper) and CSF-Cur (bottom) conjugates.

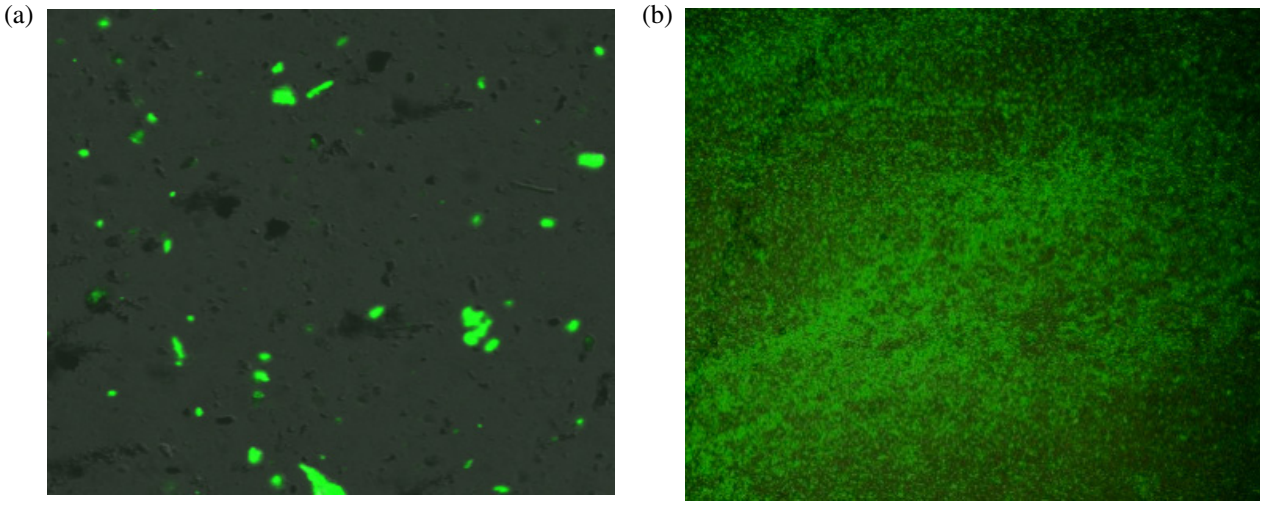

Figure 5. Confocal microscope images of dilute Fe_3O_4/CS-Cur (a) and Fe_3O_4/OLF-Cur (b).

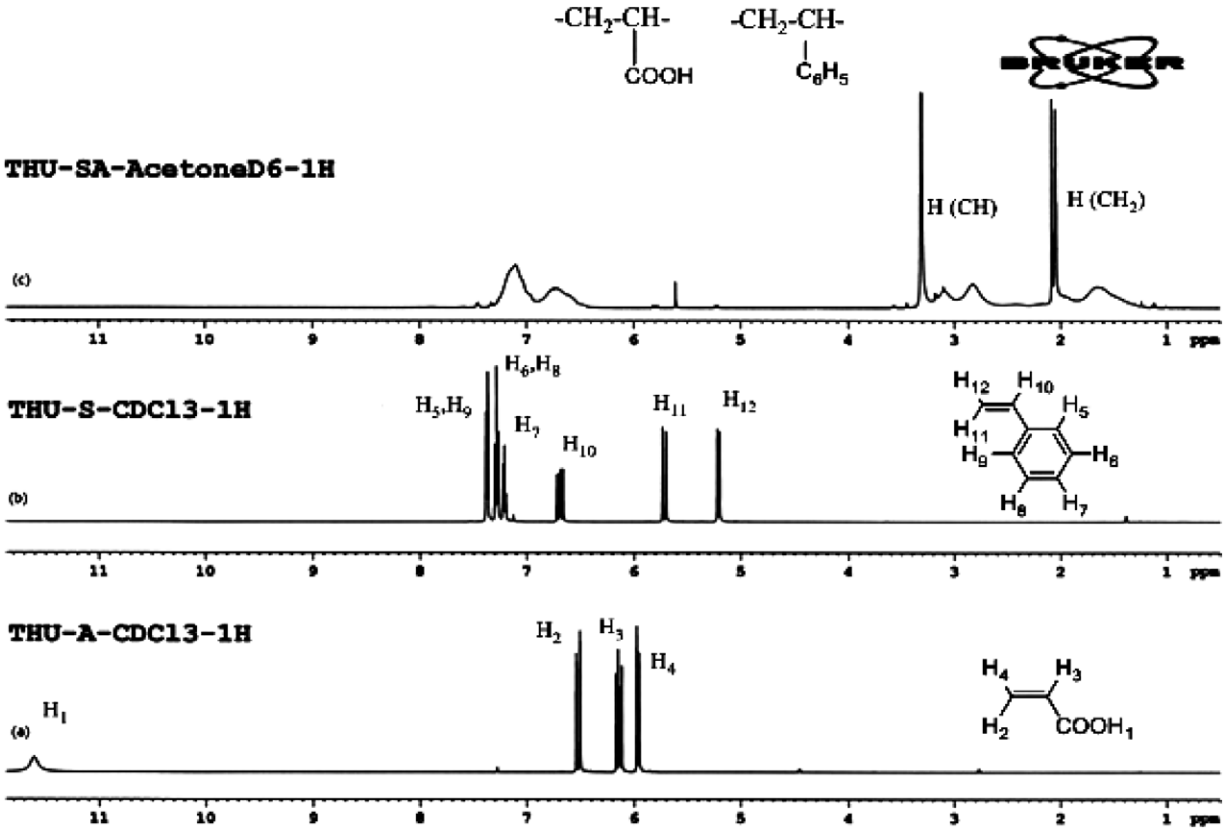

Figure 6. [1]H-NMR spectra of AA, St and poly(St-co-AA).

of CS and styrene (St) the materials serve as a matrix to catch 'the MNPs' of a much larger amount of Fe_3O_4 particles.

As one can note from figure 9 and table 1, loading of curcumin almost does not reduce the MNP concentration in the resulted complex colloids. Interestingly, as indicated in [23] for the case of OCMCS capping material, curcumin is much better adsorbed onto Fe_3O_4/OCMCS system than on OCMCS nanoparticles alone.

3.1.3. MIH performance. Typical heating curves are depicted in figure 10 for MNP conjugates capped with three different materials, namely poly(St-co-AA) (a), CS (b) and OCMCS (c). For each conjugate the temperature versus time curves were carried out for not only the as-prepared colloidal but also for four samples of further dilution in distilled water. The saturation temperature T_s (defined as the temperature gained at heating time of $t_o = 60$ s) and specific absorption rate (SAR)

$$SAR = \frac{C}{c}\left.\frac{dT}{dt}\right|_{t=0},$$

where C and c are the specific heat and the concentration of the liquid, estimated for the as-prepared samples are gathered in table 1. As seen in table 1 and figure 10, the T_s and SAR

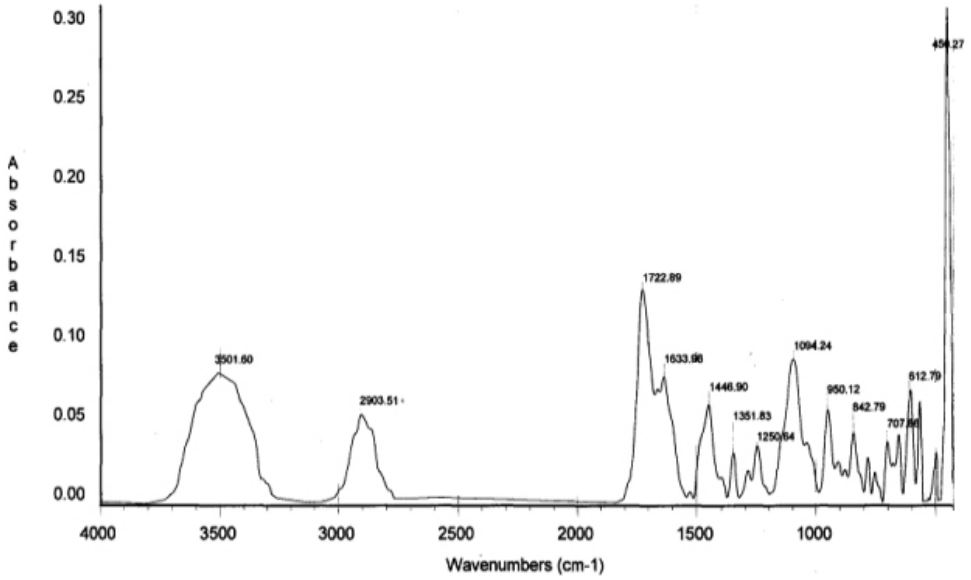

Figure 7. IR spectra of Fe_3O_4/poly(St-co-AA).

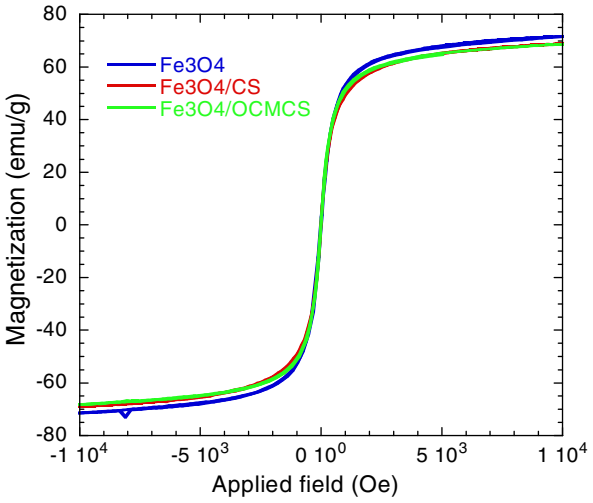

Figure 8. Magnetization of naked and (dried) CS-capped and OCMCS-capped Fe_3O_4 samples.

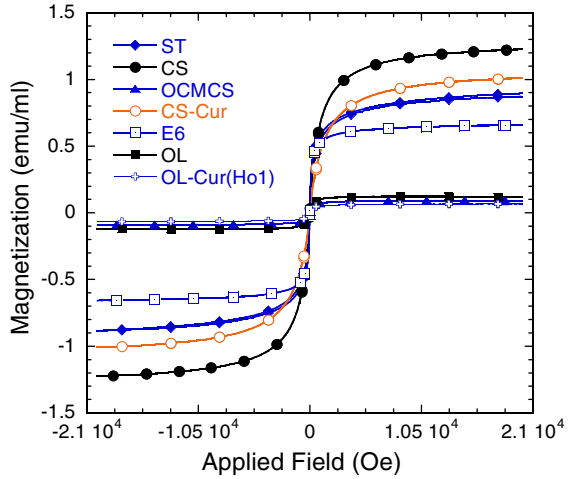

Figure 9. Magnetization of various magnetic fluid samples (see table 1 and text for abbreviations).

Table 1. Synthesized conjugates and basic characteristic parameters

Capping material	Ms (emu g^{-1})	c (mg ml^{-1})	T_s (°C)	SAR (w g^{-1})
ST	0.88	12.6	75	272
Dextran	–	10	70	55
CS	1.224	17.5	>100	840
OCMCS	1.02	14.7	98	568
CS-Cur	1.03	14.7	67	117
St-co-AA (E6)	0.64	9.14	70	540
OL	0.123	1.76	35	–
OL-Cur (Ho1)	0.125	1.77	35	–

are monotonically increased with magnetization namely the higher the magnetization the larger the energy absorbed by the MNPs. One can easily note that Fe_3O_4/poly(St-co-AA) and Fe_3O_4/OCMCS exhibit a linear dependence of the characteristic heating parameters on MNP concentration, whereas in the case of Fe_3O_4/CS there is a clear deviation from such behavior in the most dilute range. The faster decrease of SAR in that dilute concentration region of the Fe_3O_4/CS is explained [23] by the assumption of appearance of clusters or a bad solution of MNP capped by the unmodified chitosan in high pH condition (see figure 5(a)).

3.1.4. Magnetic stability. In order to verify the stability, magnetization was measured for ferrofluids diluted in various liquids, which were sealed in glass holder over several days. As shown in figure 11, the Fe_3O_4/poly(St-co-AA) diluted to the biological pH (7.3) is stable over several weeks and the Fe_3O_4/OL-Cur diluted in physiological liquid can remain stable for at least one week. These characteristics show that the fabricated conjugates are stable enough to be used for *in vitro* and *in vivo* treatments.

3.1.5. Toxicity of the ferrofluids. Toxicity of the ferrofluids was tested via determination of half maximal inhibitory concentration (IC_{50}) or/and of cytotoxicity index

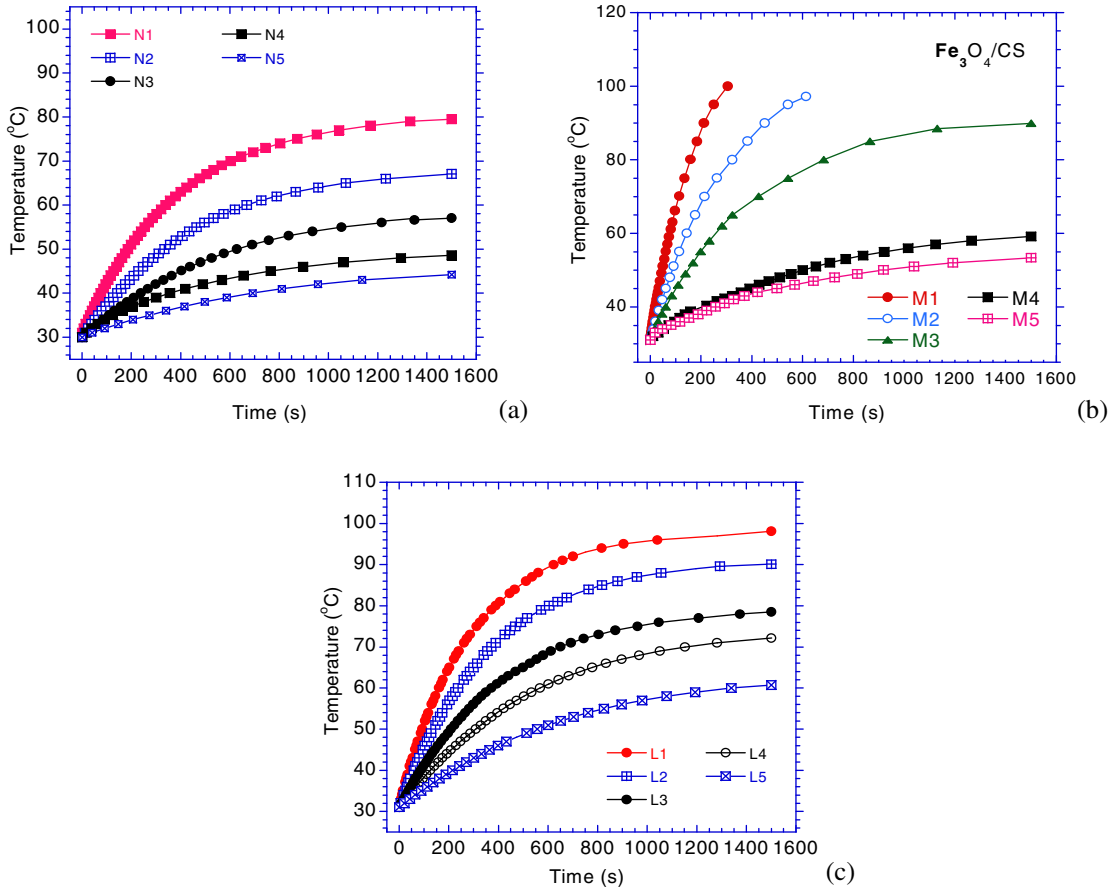

Figure 10. Magnetic heating curves measured at various concentrations for (a) Fe_3O_4/poly(St-co-AA), (b) Fe_3O_4/CS and (c) Fe_3O_4/OCMCS.

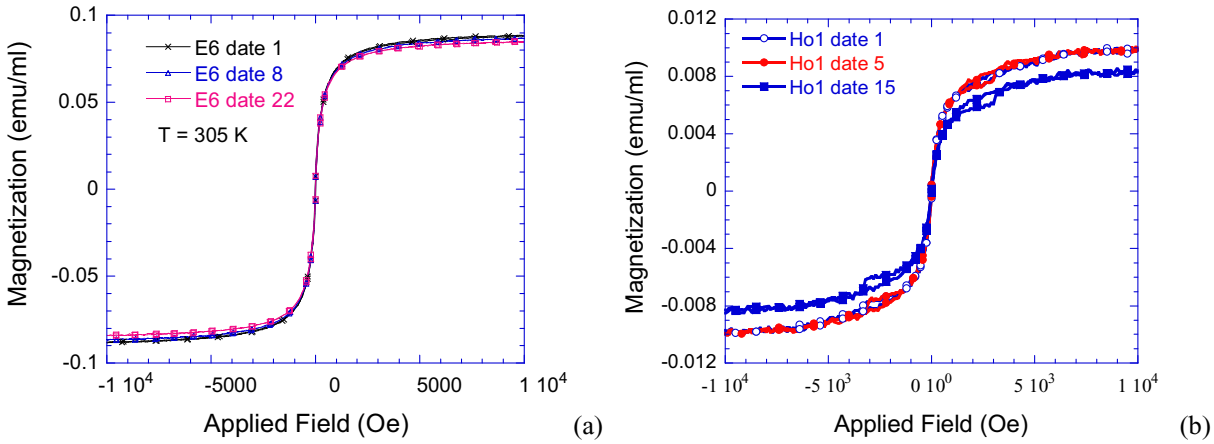

Figure 11. Stability of Fe_3O_4/poly(St-co-AA) suspension in water (a), and of Fe_3O_4/OL-Cur in physiological liquid (b).

concentration causing 50% mortality (CI_{50}) of cells as affected by the conjugates. From the dose-response curves shown in figure 12, one can see that $IC_{50} > 100\,\mathrm{mg\,ml^{-1}}$ for both the ferrofluids and depending neither on the Madin Darby canine kidney (MDCK) nor Michigan Cancer Foundation-7 (MCF7) cells. For the Fe_3O_4/poly(St-co-AA) conjugate the IC_{50} was estimated to be of $20\,\mu\mathrm{g\,ml^{-1}}$ to inhibit a lung cancer cell but still safe towards other cells such as rhabdosarcoma (RD) and heptatoma (HepG2) cancer cells (table 2). The CI_{50} index of the Fe_3O_4/poly(St-co-AA) towards HepG2 and fibroblast cells were found to be of 0.5 and $1.0\,\mathrm{ng^{-1}cell}$, respectively, and these values are around two times larger than those of the Fe_3O_4/OL-Cur conjugate.

3.2. Hyperthermia treatment of mice

3.2.1. In vitro *observation of killing of cancer cells.* *In vitro* experiments were performed for treatment of Sarcoma 180 cancer cells with the use of two conjugates, namely the MNP capped by starch and poly(St-co-AA). From the heating characterization curves (figure 10(a)) proper MNP concentrations, c_o, to create the temperature for killing cancer cells (45–49 °C) were chosen. Liquid samples of

Table 2. The proliferation of three cancer cell lines (HepG2, Lu and RD) treated with Fe_3O_4/CS and Fe_3O_4/OCMCS.

	Cell lines Cell survival (%)			
Sample	HepG2	Lu	RD	Result
DMSO	100.0 ± 0.0	100.0 ± 0.0	100.0 ± 0.0	
Ref(+)	1.8 ±0.05	1.2 ±0.1	0.5 ±0.06	+
Fe_3O_4/CS	97.4 ±0.3	78.2 ±0.7	92.7 ±0.8	−
Fe_3O_4/OCMCS	92.7 ±0.5	96.7 ±1.1	99.5 ±0.09	−
E6	63.0 ±0.8	50.1 ±0.2	83.8 ±0.4	+ for Lu; − for HepG2 and RD

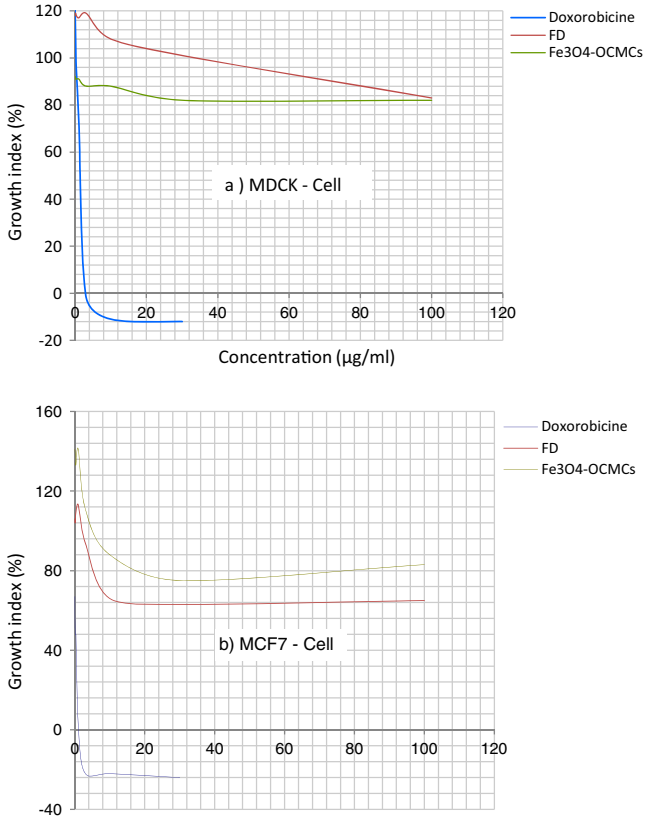

Figure 12. Dose-response curves of normal (kidney) cell MDCK (a) and breast cancer cell line MCF7 (b) treated with doxorobicin and dextran (FD) and OCMCS ferrofluids.

those concentrations of MNPs were prepared and inserted into a glass vessel, and the vessel together with an optical temperature sensor was introduced into the field coil (figure 1(b)). Figure 13 shows time dependence of the temperature (a), and the calculated amount of killed cells at various heating times (b) for the case of poly(St-co-AA) ferrofluid. As shown, after around 1 h of heating, the cancer cells were totally killed.

3.2.2. Ex vivo *characterization of MNP location.* *Ex vivo* experiments of measuring temperature versus time were conducted after injection of the Fe_3O_4/poly(St-co-AA) conjugate both via vein and direct injection to the solid tumor of experimental Swiss mice. The MIH measurements for the animal organs and the tumor showed that, for the first case, the MNPs turned to accumulate mostly in the liver, whereas in the latter case they remained at the tumor site for several hours. The direct injection *ex vivo* experiment was also utilized to confirm the estimated dose necessary for further *in vivo* experiments for a tumor of the same size.

3.2.3. In vivo *treatments of tumor on mice.* Table 3 presents experimental design for *in vivo* treatment of (Sarcoma) solid tumor. As indicated, five mice with solid tumor of size around $6 \times 6\,\text{mm}^2$, which was subcutaneously inoculated on Swiss mice, were chosen for each experimental series, namely three control (cancer, irradiation and ferrofluid) and two treated mice of different doses. As indicated by the photos in figure 14 (shown only for A and C mice), in all the control mice the tumor continuously increased with time and the mice died at around 4 weeks after starting the experiment, whereas the mice C and D treated with dose of 0.3 and 0.4 mg (per tumor of $6 \times 6\,\text{mm}^2$ size) were totally recovered 3 weeks after three courses of irradiation during the first week. The treatment efficacy was evidenced by shrinking of the tumor even after the first course of irradiation by the ac magnetic field.

3.3. Fluorescence imaging and magnetic imaging characteristics

3.3.1. Fluorescence study of MNPs uptake by macrophage. Figure 15 presents confocal image of the macrophages before (a) and after its uptake with Fe_3O_4/CS-Cur (b), and Fe_3O_4/OL-Cur (c) ferrofluids. With the blue and green colors marked respectively for the cellular nucleus and Cur accumulated in vacuole, one can clearly see that the uptaken conjugates, evidenced by green spots of the Cur, are situated in the latter part of the cells. Such occupation of the Fe_3O_4-based conjugates is confirmed also by TEM imaging as demonstrated in figure 16 for the case of Fe_3O_4/OL-Cur. Comparing the two techniques one can deduce that the presence of Cur has created a wonderful enhancement in contrast of the imaging technique even at cellular level (see also [24] for the case of Fe_3O_4 coated by OCMCS with human colon adenocarcinoma (HT29) cancer cells.

3.3.2. Fluorescence and magnetization studies of uptake kinetics. With such good contrast enhancement and monodisperse behavior in physiological condition the Fe_3O_4/OL-Cur was then used for studying kinetics of the conjugate uptake into macrophage. As shown in figure 17, the number of Fe_3O_4/OL-Cur conjugates uptaken into cell cytoplasm increases with increasing incubation time. This effect was confirmed also by PPMS magnetization measurements for the samples interrupted at 1, 2, 4 and 6 h (figure 18).

Table 3. Designed series of experimental mice for *in-vivo* MIH hyperthermia.

Mouse	Tumor size (mm^2)	Amount of ferrofluid injected (μg)	Period of irradiation (min)	Number of treatments
A Contr.	6.0×6.0	0	0	0
B Contr.	6.0×6.5	0	30	3
C Treat.	5.5×6.0	300	30	3
D Treat.	6.5×6.5	400	30	3
E Contr.	6.0×6.0	400	0	0

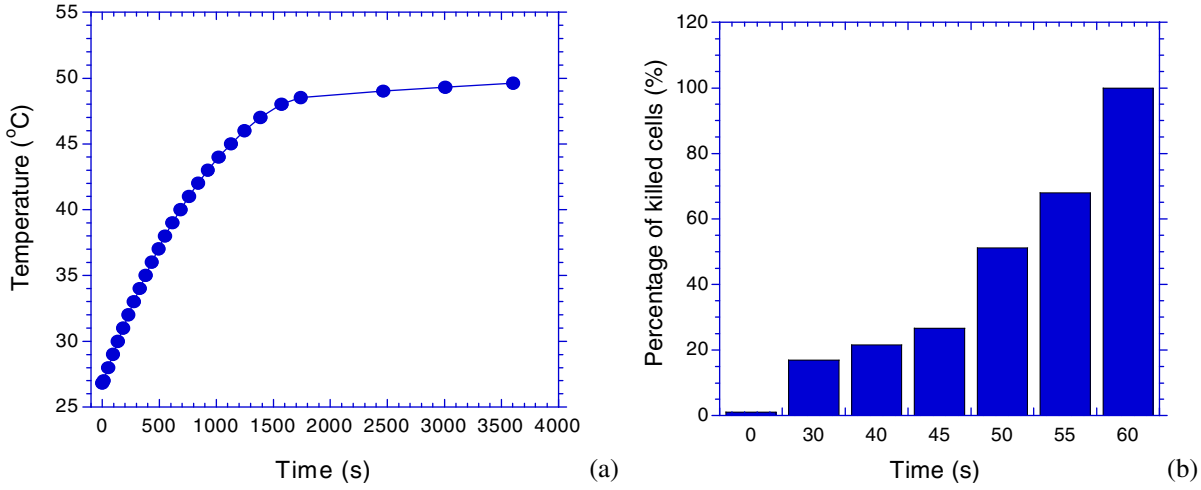

Figure 13. *In vitro* experiment with use of Fe_3O_4/poly(St-co-AA). (a) Time dependence of the temperature and (b) relative number of killed cells at various times.

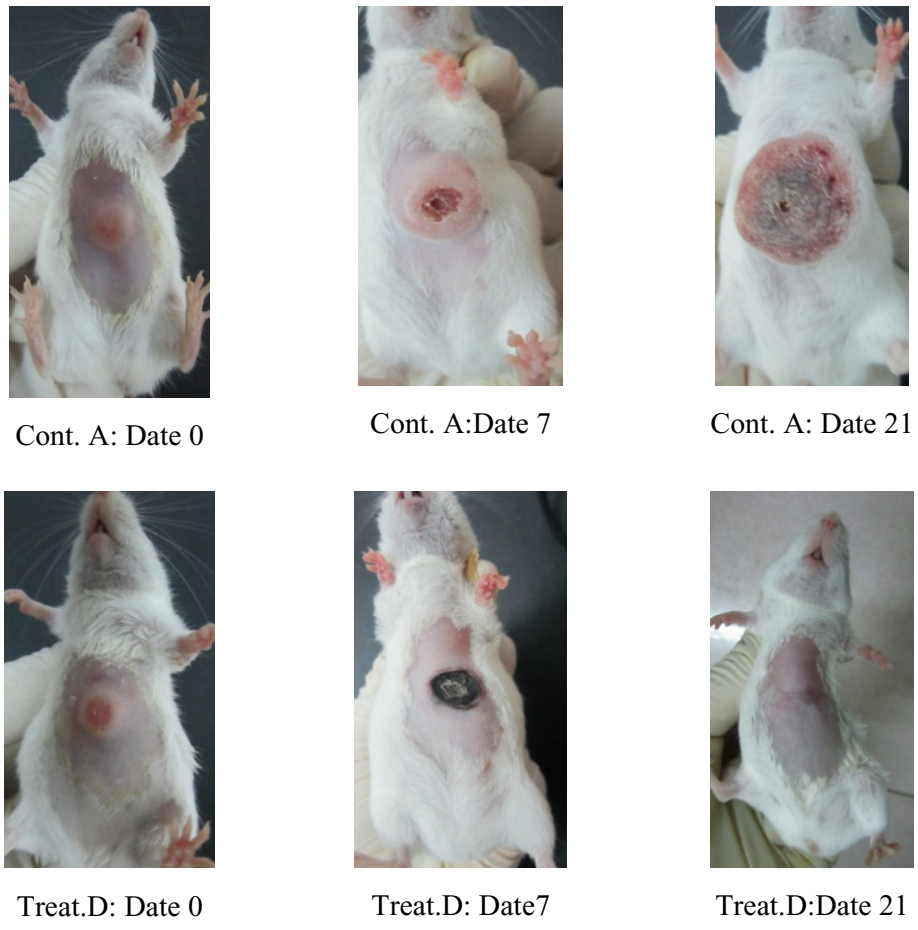

Figure 14. Images of the two mice of control A (top) and treated D (bottom) mice at three date periods. Ferrofluid used: Fe_3O_4/poly(St-co-AA).

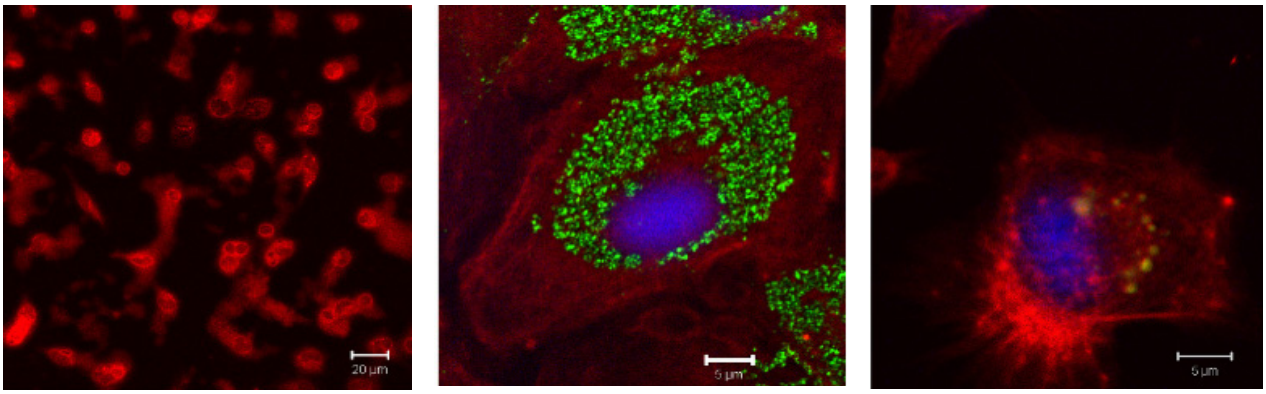

(a) (b) (c)

Figure 15. Fluorescence images of monocyte-derived macrophage stained for CD14 (a), phagocytosis of human macrophage with CSF (b) and mouse macrophage with OLF (c).

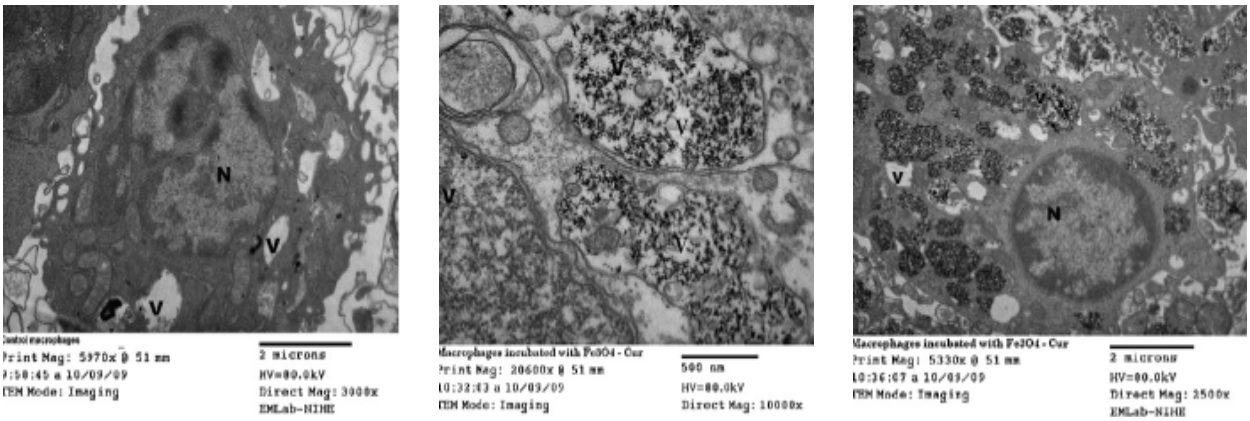

(a) (b) (c)

Figure 16. TEM images of mouse macrophage before (a) and after (b, c) OLF-Cur uptake.

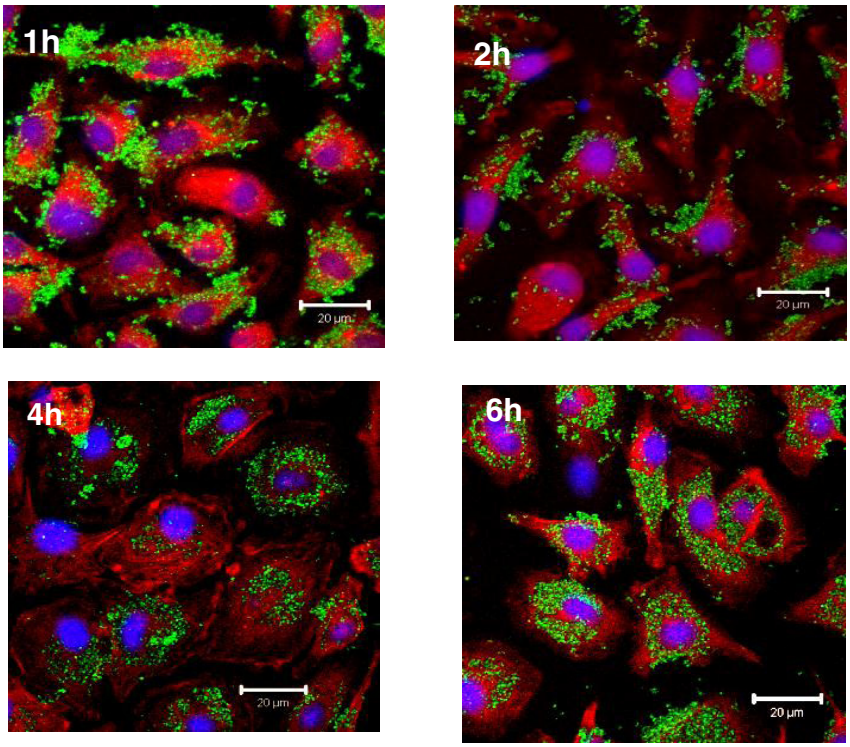

Figure 17. Confocal fluorescence images: *in-situ* observation of Fe_3O_4/OL-Cur uptake by macrophage.

Table 4. MRI *in vitro* experiment of MNP uploaded macrophage. Res denotes ferrofluid.

5×10^5cells Res/4 h (1)	5×10^5cells Ho1/4 h (2)	10^7cells Res/4 h (3)	10^7cells Ho1/4 h (4)		
10^6cells (5)	10^6cells Ho1/2 h (6)	10^6cells Res/2 h (7)	10^6cells Ho1/4 h (8)	10^6cells Res/4 h (9)	Agarose

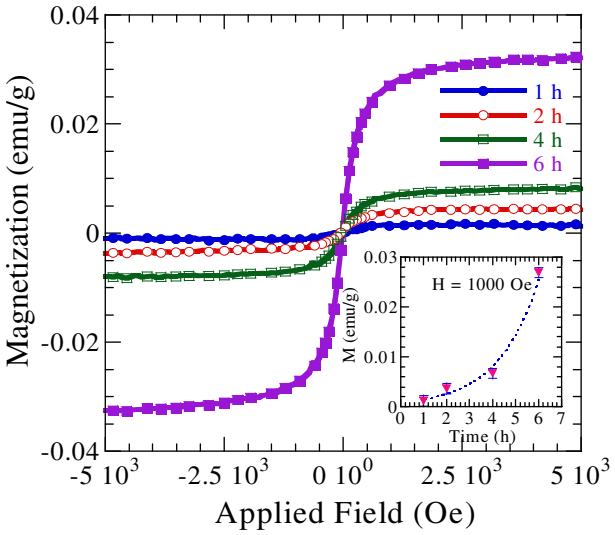

Figure 18. Magnetization of macrophages uptaking with Fe_3O_4/OL-Cur at various times.

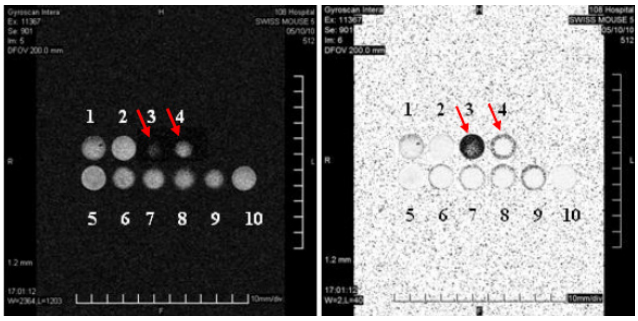

Figure 19. MRI images for MNPs- uptaken macrophages (see table 4 for particular wells).

3.3.3. MRI imaging. With the aim of using macrophage as vehicles to carry contrast enhancer into tumors we studied if there was any influence of the carrier on the contrast behavior. This *in vitro* experiment was designed with the use of a 12 wells array for the Fe_3O_4/OL-Cur ferrofluid (Ho1 sample) and a commercial agent Resovist (Res). After incubation of macrophage with the ferrofluids, the uptaken cells were calculated and delivered to the wells as shown in table 4. The T_2-weighted MRI images of the wells are presented in figure 19. As seen, except for wells 5 and 10 (without MNPs) all other samples exhibit contrast enhancement. By comparison of wells 3 and 4, of best contrasts, one can easily see much better performance of the former case. This contrast difference is explained by the more than one order difference of the MNP concentrations of the ferrofluid used for the

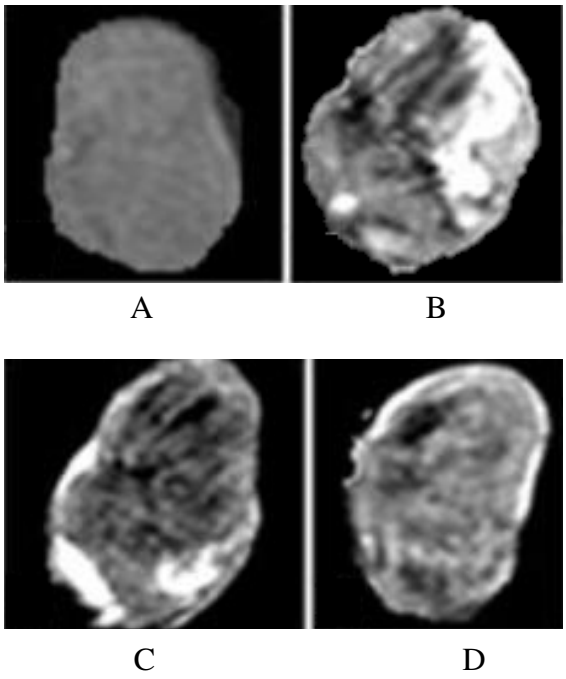

Fgure 20. MRI (*ex vivo*) images for tumors injected by Ho1-uptaken macrophages. (A): Cancer control, (B): direct injected, (C): vein injected, (D): vein injected, magnet attract.

two wells, i.e. $c(\text{Resovist}) = 28\,\text{mg ml}^{-1}$, while $c(\text{Ho1}) = 1.7\,\text{mg ml}^{-1}$. Having concluded that the macrophages do not interfere with the MRI contrast of the ferrofluid, we then used the MNP loaded macrophages to inject into Swiss mice. Figure 20 shows the MRI (*ex vivo*) images for tumors injected by the Ho1-uptaken macrophages. As clearly seen, differently from the cancer control mouse (A), all other ferrofluid-injected mice exhibit detailed structures of the tumor images. While the appearance of MNPs (black stripes and spots) in tumor for the case of direct injection (B) sounds obvious (as observed also in the MIH study described in section 2), the accumulation of MNPs in tumor for the case of vein injection is quite a new observation, which was not clearly evidenced by that MIH research. We therefore assume this evidence to be related to the biological tendency of the macrophage to penetrate into the tumor interior [25].

4. Conclusion

From the research presented above, one can summarize that: (i) various magnetite-based conjugates have been successfully fabricated, that appear to be sufficiently stable and biocompatible for further biomedical applications; (ii) copolymer conjugate of Fe_3O_4/poly(St-co-AA) has been proved to be physiologically stable, with high MIH performance, and a good candidate for hyperthermia agent; (iii) the Cur-loaded Fe_3O_4/OL conjugate exhibits strong fluorescence, which makes it a good candidate for a multimodal (fluorescent and MRI) imaging agent, although further investigation needs to be done to enhance its magnetization; (iv) macrophage was shown up to be a potential vehicle for carrying MRI and fluorescence agent into tumor.

Acknowledgments

The authors are indebted in acknowledging the financial support mainly from the MOST grant no. 4/2/742/2009-HD-DTDL and partly from a research grant of VAST for the 2009–2010 period. Sincere thanks are due to Professor Academician Nguyen Van Hieu for his encouragement in doing such a new and interdisciplinary research.

References

[1] Ferrieri M 2005 *Nature Rev. Cancer* **5** 161
Brigger I, Dubernet C and Couvreur P 2002 *Adv. Drug Deliv. Rev.* **54** 63
[2] Shubayev V, Pisanic T R and Jin S H 2009 *Adv. Drug Rev.* **61** 467
[3] Takae S, Akiyama Y, Otsuka H, Nakamura T, Nagasaki Y and Kataoka K 2005 *Biomacromol.* **6** 818
[4] Panchurst Q A, Connolly J, Jones S K and Dobson J 2003 *J. Phys. D: Appl. Phys.* **36** R167
Pankhurst Q A, Thanh N K T, Jones S K and Dobson J 2009 *J. Phys. D: Appl. Phys.* **42** 4001
[5] Moenet S, Vasseur S, Grasset F and Duguet E 2004 *J. Mater. Chem.* **14** 2161
[6] Gupta A K and Gupta M 2005 *Biomaterials* **26** 3995
[7] Lu A H, Salabas E L and Schulth F 2007 *Angew Chem., Int. Ed. Engl.* **46** 1222
[8] Lee J-H, Jiang J-T, Choi J-S, Moon S H, Noh S-H, Kim J-W, Kim J-G, Park K I and Cheon J 2011 *Nature Nanotechnol.* **6** 418
[9] Park J K, Jung J, Subramania P, Shah B P, Kim C, Lee J K, Cho J H, Lee C and Lee K-B 2011 *Small* **7** 1647
[10] Pantic I 2010 *Rev. Adv. Mater. Sci.* **26** 67
[11] Lacroix L-M, Ho D and Sun S 2010 *Curr. Top. Med. Chem.* **10** 1184
[12] Wang Y-X J, Hussain S M and Krestin G P 2001 *Eur. Radiol.* **11** 2319
[13] Prashant C, Dipak M, Yang C-T, Chuang K-H, Jun D and Feng S-S 2010 *Biomaterials* **31** 5588
[14] Yanase M, Shinkai M, Honda H, Wakabayashi T, Yoshida J and Kobayashi T 1998 *Japan. J. Cancer Res.* **89** 463
Ito A, Shinkai M, Honda H and Kobayashi T 2001 *Cancer Gene Ther.* **8** 649
[15] Brusentsov N A, Nikitin L V, Brusentsova T N, Kuznetsov A A, Bayburskiy F S, Shumakov L I and Jurchenko N Y 2002 *J. Magn. Magn. Mater.* **252** 378
[16] Gneveckow U, Jordan A, Scholz R, Brub V, Waldofner N, Ricke J, Feussner A, Hildebrant B, Rau B and Wust P 2004 *Med. Phys.* **31** 1444
[17] Hilger I, Hergt R and Kaiser W A 2005 *IEE Proc.—Nanotechnol.* **152** 33
[18] Pham H L, Do H M, Tran D L, Le V H, Nguyen X P, Nguyen A T, Nguyen T N and Vu A T 2011 *Int. J. Nanotechnol.* **8** 399
[19] Pham H L, Nguyen C T, Nguyen A T, Pham V T, Tran C Y, Nguyen T Q, Hoang T M N, Phi T X, Nguyen X P and Le V H 2009 *J. Phys.: Conf. Series* **187** 012008
[20] Ha P T, Tran T M N, Pham H D, Nguyen Q H and Nguyen X P 2010 *Adv. Nature. Sci.: Nanosci Nanotechnol.* **1** 015012
[21] Tran D L *et al* 2010 *Colloid. Surf.* A **371** 104
[22] Luong T T *et al* 2011 *Colloid. Surf.* A **384** 23
[23] Mai T T, Ha P T, Pham H N, Le T T H, Pham H L, Phan T B H, Tran D L and Nguyen X P 2012 *Adv. Nature Sci.: Nanosci. Nanotechnol.* **3** 015006
[24] Ha P T *et al* 2011 *Chem. Lett.* **40** 1264
[25] Muthana M, Scott S D, Farrow M, Morrow F, Murdoch C, Grubb S, Brown N, Dobson J and Lewis C E 2008 *Gene Ther.* **15** 902